AGU PUBLICATIONS

JGR

Journal of Geophysical Research: Atmospheres

RESEARCH ARTICLE
10.1002/2016JD025946

Key Points:
- Spaceborne lidar partitions global total cloud cover into 35% thin and 31% opaque
- The lidar attenuation altitude directly controls TOA longwave emission by opaque clouds
- Simulator-enabled comparisons reveal large compensating climate model errors with relevance to circulation and feedback

Correspondence to:
R. Guzman,
rodrigo.guzman@lmd.polytechnique.fr

Citation:
Guzman, R., H. Chepfer, V. Noel, T. Vaillant de Guélis, J. E. Kay, P. Raberanto, G. Cesana, M. A. Vaughan, and D. M. Winker (2017), Direct atmosphere opacity observations from CALIPSO provide new constraints on cloud-radiation interactions, *J. Geophys. Res. Atmos.*, *122*, 1066–1085, doi:10.1002/2016JD025946.

Received 16 SEP 2016
Accepted 31 DEC 2016
Accepted article online 4 JAN 2017
Published online 19 JAN 2017

Direct atmosphere opacity observations from CALIPSO provide new constraints on cloud-radiation interactions

R. Guzman[1], H. Chepfer[2], V. Noel[3], T. Vaillant de Guélis[2], J. E. Kay[4], P. Raberanto[1], G. Cesana[5], M. A. Vaughan[6], and D. M. Winker[6]

[1]LMD/IPSL, CNRS, Ecole Polytechnique, Palaiseau, France, [2]LMD/IPSL, Université Pierre et Marie Curie, Paris, France, [3]LA CNRS, Toulouse, France, [4]CIRES/ATOC, University of Colorado Boulder, Boulder, Colorado, USA, [5]JPL, California Institute of Technology, Pasadena, California, USA, [6]NASA Langley Research Center, Hampton, Virginia, USA

Abstract The spaceborne lidar CALIPSO (Cloud-Aerosol Lidar and Infrared Pathfinder Satellite Observation) directly measures atmospheric opacity. In 8 years of CALIPSO observations, we find that 69% of vertical profiles penetrate through the complete atmosphere. The remaining 31% do not reach the surface, due to opaque clouds. The global mean altitude of full attenuation of the lidar beam (z_opaque) is 3.2 km, but there are large regional variations in this altitude. Of relevance to cloud-climate studies, the annual zonal mean longwave cloud radiative effect and annual zonal mean z_opaque weighted by opaque cloud cover are highly correlated (0.94). The annual zonal mean shortwave cloud radiative effect and annual zonal mean opaque cloud cover are also correlated (−0.95). The new diagnostics introduced here are implemented within a simulator framework to enable scale-aware and definition-aware evaluation of the LMDZ5B global climate model. The evaluation shows that the model overestimates opaque cloud cover (31% obs. versus 38% model) and z_opaque (3.2 km obs. versus 5.1 km model). In contrast, the model underestimates thin cloud cover (35% obs. versus 14% model). Further assessment shows that reasonable agreement between modeled and observed longwave cloud radiative effects results from compensating errors between insufficient warming by thin clouds and excessive warming due to overestimating both z_opaque and opaque cloud cover. This work shows the power of spaceborne lidar observations to directly constrain cloud-radiation interactions in both observations and models.

1. Introduction

Climate feedback analyses reveal that clouds are a large source of uncertainty for the climate sensitivity of climate models and thus for future climate projections [e.g., *Taylor et al.*, 2007; *Webb et al.*, 2006; *Bony et al.*, 2006; *Boucher et al.*, 2013]. Boosting confidence in climate model projections requires identifying model physics deficiencies via comparison to observations [e.g., *Klein and Jakob*, 1999; *Bodas-Salcedo et al.*, 2008; *Nam et al.*, 2012; *Cesana and Chepfer*, 2012, 2013; *Marchand et al.*, 2009; *Kay et al.*, 2012; *English et al.*, 2014; *Kay et al.*, 2016a] and then improving the representation of relevant physics in the models [*Konsta et al.*, 2012; *Kay et al.*, 2011; *Kay et al.*, 2016b]. *Taylor et al.* [2012] suggest that in the analysis of the complex climate system, a useful first step is to consider the processes that are energetically dominant, since processes that weakly affect the energy flow and storage within the system are unlikely to dominate its response to perturbation.

Earth's temperature is largely driven by the balance of the fluxes of shortwave (visible) and longwave (infrared) radiation at the top of the atmosphere (TOA). In turn, global radiation balance depends on the atmospheric opacity. Clouds represent the most variable and uncertain contributor to atmospheric opacity for two reasons: (1) cloud opacity impacts both shortwave fluxes reflected back to space and outgoing longwave fluxes and (2) cloud temperature controls upwelling and downwelling longwave radiation within the atmosphere.

Knowing that cloud opacity has a large influence on global radiation budgets, we separate clouds into two distinct classes: opaque clouds and thin clouds. Opaque clouds are optically thick enough to prevent longwave radiation coming from the surface and low-level layers from reaching the TOA and to prevent direct solar radiation from reaching lower tropospheric layers, increasing the cloud albedo. Unlike opaque clouds, thin clouds are semitransparent. Thin clouds let part of the direct solar shortwave radiation penetrate down to the surface and part of the surface-emitted longwave radiation through the atmosphere up to the TOA.

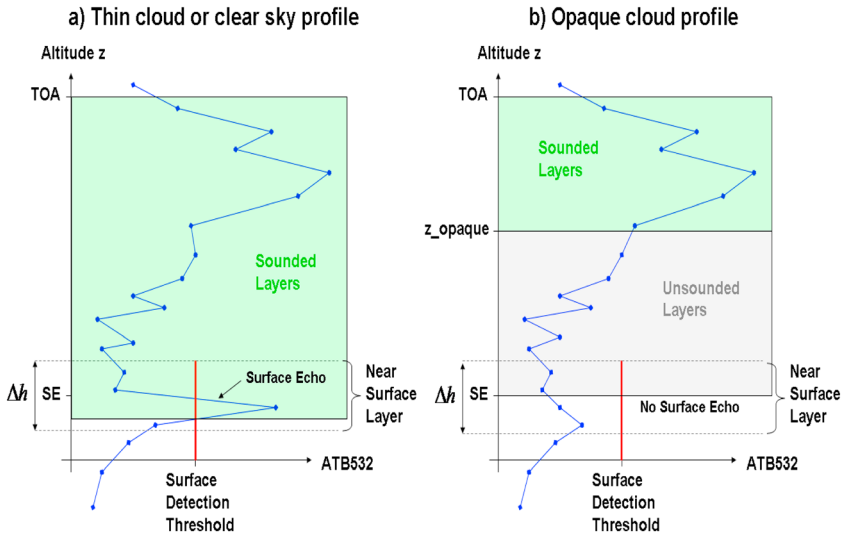

Figure 1. Surface echo detection scheme: ATB surface detection threshold (SDT) applied in a near-surface layer (NSL) extending from $-\Delta h/2$ to $+\Delta h/2$ with respect to the surface elevation (SE) for (a) a thin cloud or clear-sky profile case where the surface is detected and (b) an opaque cloud profile case where the surface is not detected.

This direct division of the total cloud cover into opaque and thin cover is new, novel, and useful for two reasons. First, opaque cloud cover is strongly linked to atmospheric radiative fluxes and TOA radiation balance. Second, opaque and thin cloud cover can be precisely detected by spaceborne lidar observations [*Martins et al.*, 2011]. The robust observation of atmospheric opacity enabled by spaceborne lidar provides new information beyond what column-integrated radiative fluxes can. The lidar measures the altitude where the atmosphere is opaque to visible radiation with an accuracy of meters. As a result, the separation of cloud cover into opaque and thin is done directly, without reliance on an optical depth retrieval with large uncertainties due to required assumptions (e.g., in cloud microphysics or surface type). More importantly, the lidar gives access, for the first time, to the height of attenuation of direct visible radiation (z_opaque). Z_opaque cannot be retrieved by passive sensors that are sensitive to vertically integrated radiative fluxes.

Z_opaque is not only the altitude where the lidar signal is fully attenuated. It can also be directly related to longwave TOA radiative fluxes. Full lidar attenuation typically corresponds to a visible cloud optical depth (τ_{VIS}) of 3 to 5 and to a cloud infrared emissivity (ε_{Cloud}) of 0.8 [*Chepfer et al.*, 2014], as cloud particles are much larger than visible wavelengths $\left(\varepsilon_{Cloud} \approx 1 - e^{-\frac{\tau_{VIS}}{2}}\right)$. Thus, z_opaque is the altitude where the longwave radiation coming from below is no longer transmitted directly upward.

Having introduced our tools and terminology, we next describe the two goals of this paper. Our first goal is to reveal how the three new cloud diagnostics, opaque cloud cover, thin cloud cover, and z_opaque, are connected to cloud-radiation interactions, by confronting their global distributions. Our second goal is, by incorporating them in a satellite simulator framework to reveal model strengths and weaknesses in climate model representations of atmospheric opacity.

The paper is organized as follows: Section 2 describes the algorithm that generates the three new cloud diagnostics. Section 3 describes how this algorithm is implemented within the lidar simulator [*Chepfer et al.*, 2008] included in the Cloud Feedback Model Intercomparison Project (CFMIP) Observation Simulator Package (COSP) [*Bodas-Salcedo et al.*, 2011]. Section 4 shows global maps of our three new cloud diagnostics both from observations and within a climate model. Finally, section 5 draws conclusions and perspectives emerging from the new diagnostics presented in this paper.

2. Observations of Cloud Opacity With CALIPSO: The OPAQ Algorithm

Here we describe how the OPAQ algorithm works. First it identifies opaque and thin clouds in individual General Circulation Model-Oriented CALIPSO Cloud Product (GOCCP) profiles [*Chepfer et al.*, 2010]. Then it

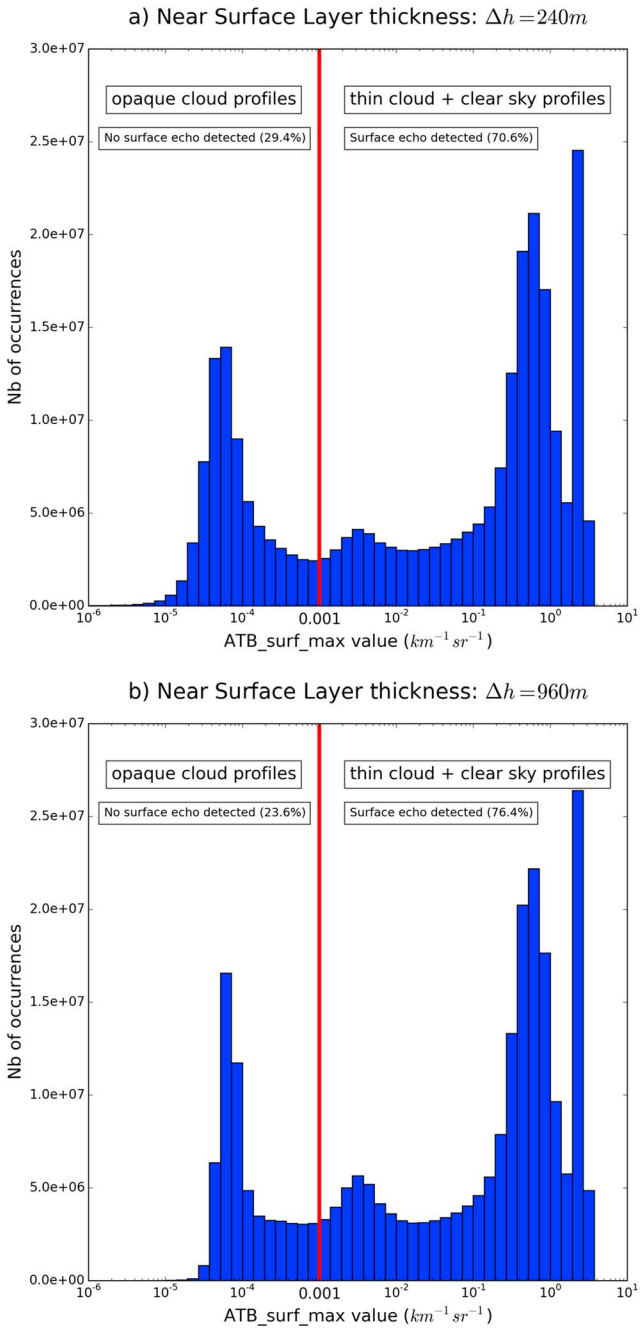

Figure 2. Distribution of the maximum ATB532 value at 30 m vertical resolution observed within near-surface layers for (a) $\Delta h = 240$ m and (b) $\Delta h = 960$ m.

finds the altitude of full opacity, termed z_opaque, key feature of the opaque cloud profile. We end this section with two examples of orbit files resulting from this processing.

2.1. When and Where Does the Lidar Profile the Complete Atmosphere?

2.1.1. Surface Detection Scheme

The OPAQ algorithm ingests individual profiles of Level 1 Total Attenuated Backscatter lidar signal at 532 nm (ATB532). The ATB532 signal has a vertical resolution of 30 m below 8.2 km above sea level (asl) and an horizontal resolution of 333 m with a 90 m diameter footprint at ground level [*Winker et al.*, 2009]. In those profiles, it first seeks the "surface echo" which corresponds to the reflection of the lidar beam when a fraction

Table 1. Percentages of Opaque Cloud Profiles and Thin Cloud + Clear-Sky Profiles for Two Near-Surface Layer Thicknesses (Δh) Using a Surface Detection Threshold = 0.001 km^{-1} sr^{-1} for All Nighttime 2012 Profiles

	Opaque Cloud Profiles	Thin Cloud + Clear-Sky Profiles
Δh	No Surface Echo: ATB_surf_max < 0.001	Surface Echo Detected: ATB_surf_max > 0.001
960 m	23.6%	76.4%
240 m	29.4%	70.6%

of its pulse reaches the surface and is reflected back to the satellite telescope. This echo is expected near the surface elevation of the lidar profile geographic location, which is provided as part of the Cloud-Aerosol Lidar with Orthogonal Polarization (CALIOP) Level 1 geolocation data and obtained from the Global 30 Arc-Second Elevation Digital Elevation Model (United States Geological Survey). As an example, Figure 1a shows a clear surface echo near the surface elevation altitude in a schematic lidar profile. This situation corresponds to a thin cloud or clear-sky atmosphere, since the visible light reaches the surface. When no surface echo spike emerges near the base of the ATB532 profile (Figure 1b), the atmospheric profile is considered as containing an opaque cloud, because the visible light has been scattered completely before reaching the surface. Nevertheless, we acknowledge the limit of the opaque cloud definition for this instrument raised by *Leahy et al*. [2012]: clouds may appear to be thin clouds either because they are truly optically thin or because the beam (~90 m of diameter every 330 m along track) falls on the edge of an opaque cloud (so part of the beam is attenuated and part is transmitted).

2.1.2. Near-Surface Layer and Surface Detection Threshold

Our systematic detection of the surface echo, required to determine if a profile contains an opaque cloud, is based on two key elements:

1. The near-surface layer extent (NSL; horizontal dashed lines in Figures 1a and 1b) is the altitude range around the expected surface elevation in which the surface spike is sought. The thickness of the NSL needs to be a multiple of the 30 m CALIOP near-ground nominal vertical resolution, and it needs to be larger than the uncertainty on the surface elevation. Here we considered NSL of 240 and 960 m.
2. The surface detection threshold (SDT; red vertical line in Figures 1a and 1b) is the minimum ATB532 value that can be attributed to a proper surface echo in the NSL. The SDT is deduced from the distribution of all the near-surface maximum ATB532 (ATB_surf_max) values observed in the NSL (Figure 2).

Figure 2a shows the ATB_surf_max distribution for NSL = 240 m. We divided this distribution in two categories. The first contains profiles with ATB_surf_max < 0.001 km^{-1} sr^{-1}; they present no surface echo and hence are associated to opaque cloud profiles. These represent 29.4% of all profiles (Table 1). The second category contains profiles with ATB_surf_max > 0.001 km^{-1} sr^{-1}; they detect surface echoes, so they correspond to profiles containing thin clouds or clear sky, but no opaque clouds. This second category contains 70.6% of all profiles (Table 1). In this category we identify a transition zone corresponding to weak surface echoes (0.001 < ATB_surf_max < 0.1), moderate surface echoes (0.1 < ATB_surf_max < 2), and strong surface echoes (ATB_surf_max > 2). Further analysis shows that strong surface echoes are only generated by ice and snow surfaces (not shown). Through the rest of this paper, we use SDT = 0.001 km^{-1} sr^{-1} for separating opaque cloud profiles from the other profiles containing clear sky or thin clouds.

We examined the sensitivity of the ATB_surf_max distribution to the thickness of the NSL by using NSL = 960 m (Figure 2b) instead of 240 m (Figure 2a) and found similar conclusions: SDT = 0.001 km^{-1} sr^{-1} is well suited to separate opaque cloud profiles from thin cloud/clear profiles in nighttime conditions. Additional analysis regarding the robustness of this threshold are given in Appendix A.

Roughly 70% of atmospheric profiles are completely sounded by the lidar (Table 1) and classified as thin cloud or clear-sky profiles. This is consistent with results from *Kato et al*. [2010] who examined the cloud bases observed by CALIPSO. Regarding the profiles containing opaque clouds, *Cesana et al*. [2016] showed that the definition of where the lidar signal is fully attenuated differs significantly among the three major CALIPSO cloud products: CALIPSO-ST [*Vaughan et al*., 2009], Kyushu [*Yoshida et al*., 2010], and GOCCP v2.9 [*Chepfer et al*., 2010]. This is due to differences in the design of each algorithm, whose development was driven by different science objectives. However, a careful consistent-definition comparison between CALIPSO-ST surface detection scheme at 532 nm and the present surface detection algorithm for all nighttime profiles of

Table 2. Definition and Characteristics of the New GOCCP v3.0 Variables Obtained From the OPAQ Algorithm

Variable	Spatial Resolution	Definition
Opaque cloud cover map	2° × 2°	Number of profiles containing at least one FA[a] layer, divided by the total number of valid profiles
Thin cloud cover map	2° × 2°	Number of profiles containing at least one cloud layer and no FA layer, divided by the total number of valid profiles
Clear sky cover map	2° × 2°	Number of profiles containing no cloud layer and no FA layer, divided by the total number of valid profiles
Z_opaque map	2° × 2°	Sum of all z_opaque values, divided by the number of opaque cloud profiles
3-D opaque cloud fraction	2° × 2° × 480 m	Sum of cloud detections at a given level of altitude in opaque cloud profiles, divided by the number of valid values, excluding FA layers, at this same level of altitude
3-D thin cloud fraction	2° × 2° × 480 m	Sum of cloud detections at a given level of altitude in thin cloud profiles, divided by the number of valid values, excluding FA layers, at this same level of altitude
3-D z_opaque fraction	2° × 2° × 480 m	Sum of z_opaque occurrences at a given level of altitude, divided by the number of valid values at this same level of altitude

[a]FA: fully attenuated.

April 2008 (~24 million profiles) gives the following figures: 30% of no surface detection for CALIPSO-ST against 29% of no surface echo for the OPAQ algorithm.

2.2. CALIPSO Full Opacity Altitude: z_opaque

The just-described surface detection scheme lets us determine when the atmosphere is only partially sounded. For these opaque cloud profiles, we define z_opaque, the altitude below which the lidar does not document the atmosphere. In such profiles, we locate z_opaque at the level just below the lowest opaque cloud layer detected in the profile. If the lowest opaque cloud layer is located at the lowest atmospheric layer of the profile, z_opaque is not declared. We use the GOCCP framework for this, which marks a cloud present when the scattering ratio (SR) is larger than 5 [*Chepfer et al.*, 2010]. GOCCP derives SR profiles from CALIOP Level 1 ATB532 profiles reprojected on a 480 m vertical grid. Hence, z_opaque is a 480 m thick layer with its center always located 480 m below the center of the lowest cloud layer ($SR > 5$) detected by GOCCP for each profile with no surface echo.

2.3. Implementation of the OPAQ Algorithm Within GOCCP

This section sums up the implementation of the OPAQ algorithm in the GOCCP v3.0 code. First, the full vertical resolution (30 m) ATB Level 1 CALIOP profile is analyzed near the surface. To do so, eight layers of the ATB532 signal are kept below and above the surface elevation given by the digital elevation model provided in CALIPSO Level 1 data set, corresponding to a 240 m thick NSL. From top to bottom of the NSL, the surface elevation is found between the fourth and the fifth layer midaltitudes, giving an atmospheric layer above the surface elevation always greater than 105 m and smaller than 135 m. In this 240 m NSL, a surface echo is detected if the $ATB\_surf\_max > SDT$, in which case the profile is not flagged as an opaque cloud profile. If $ATB\_surf\_max < SDT$ value in the NSL, the profile is flagged as an opaque cloud profile. Finally, if the surface elevation is not available, the flag is set to its fill value.

This new "surf_OPAQ" flag is combined with the legacy "Instant_Cloud" mask included in GOCCP v2.9 to build the new "Instant_OPAQ" mask included in GOCCP v3.0. Within each CALIPSO profile, the legacy Instant_Cloud mask classifies each 480 m thick atmospheric layer as cloud ($SR > 5$), uncertain ($1.2 < SR < 5$, faint cloud or aerosol layer), clear sky ($0.01 < SR < 1.2$), or fully attenuated ($SR < 0.01$) depending on its SR value.

The new Instant_OPAQ mask differs from the legacy Instant_Cloud mask as follows:

1. The SR threshold to separate the clear-sky layer and the fully attenuated (FA) layer was set to 0.01 in the legacy Instant_Cloud mask, and it is now set to 0.06 in the new Instant_OPAQ mask (justification given in Appendix C).
2. The layer just below the lowest cloud detected ($SR > 5$) is now flagged "z_opaque" for opaque cloud profiles only.

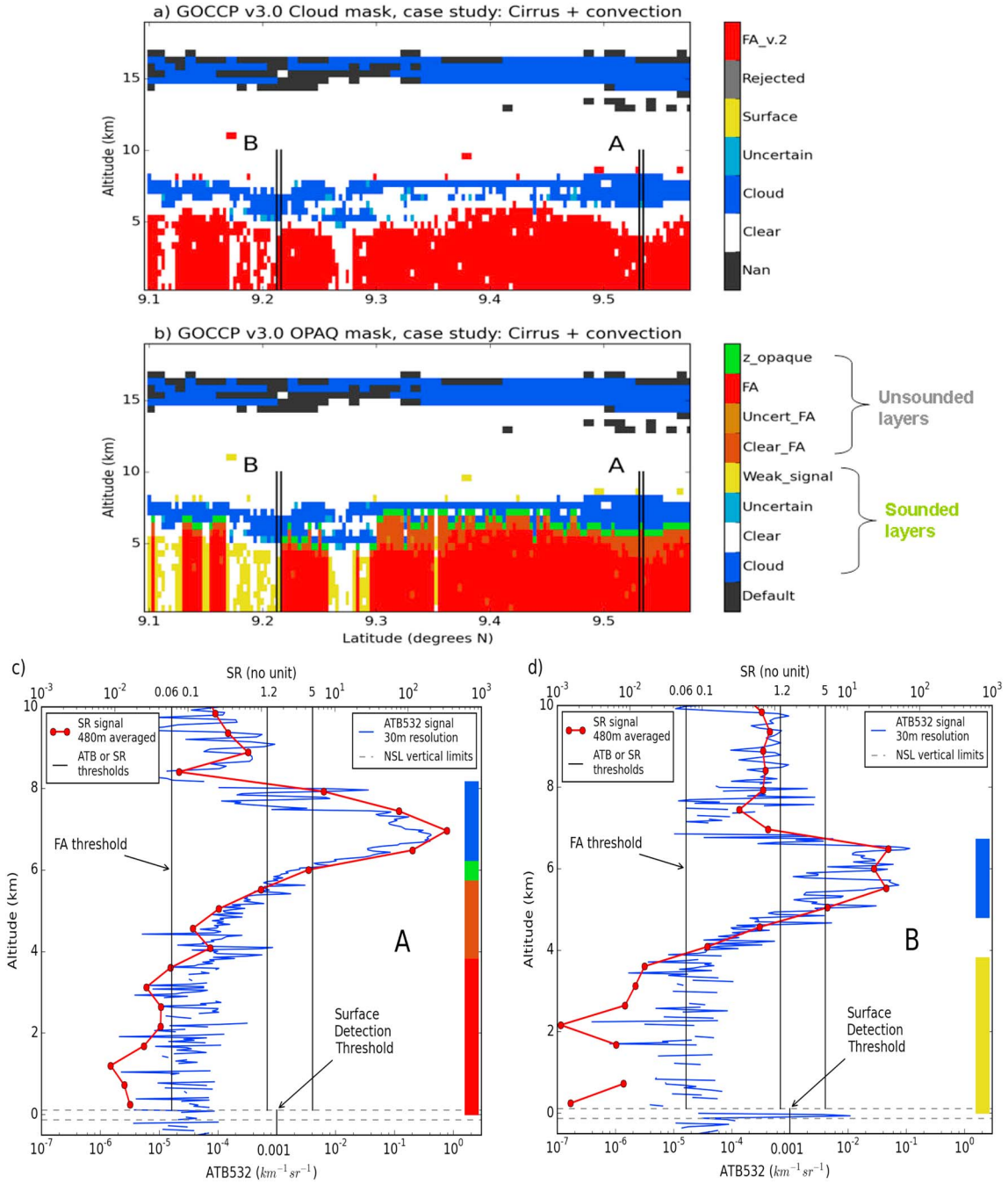

Figure 3. Level 2 masks for a Cirrus + Convection case in the Indian Ocean: (a) GOCCP v3.0 instant_Cloud_OPAQ mask and (b) GOCCP v3.0 instant_OPAQ mask. (c and d) ATB532 profiles (blue) are at 30 m vertical resolution and SR profiles (red) at 480 m vertical resolution. 15 June 2007, orbit T20-42-00ZN, A is the profile number 15454 (9.5339°N, 73.7614°E) and B is the number 15560 (9.2157°N, 73.6926°E). The vertical black lines indicate the opaque cloud profile A where the surface echo is not detected (shown in Figure 3c) and the thin cloud profile B where the surface echo is detected (shown in Figure 3d).

3. Below z_opaque, all layers are now considered as fully attenuated (FA).
4. The FA layers are now split into three subcategories: FA ($SR < 0.06$), Clear_FA ($0.06 < SR < 1.2$), and Uncert_FA ($1.2 < SR < 5$), allowing a straightforward link with the Instant_Cloud classification.

After applying the Instant_OPAQ mask to each single CALIPSO profile, a GOCCP v3.0 level 3 gridded product is built by aggregating profile information within 2° by 2° boxes. Table 2 described the new daily variables in GOCCP v3.0 compared to GOCCP v2.9. Monthly means are then calculated for both maps and 3-D variables by averaging the valid daily values.

2.4. Results for Orbit Files

2.4.1. Tropical Case Study

The first case study (Figure 3) is a segment of the 15 June 2007 nighttime orbit (T20-42-00ZN) off the South coast of India.

Figure 3a shows the "Instant_Cloud_OPAQ" mask found in GOCCP v3.0, which is exactly the same than the GOCCP v2.9 Instant_Cloud mask with just one difference: the fully attenuated (FA) layers now correspond to SR < 0.06, instead of SR < 0.01. In this updated legacy mask, most of the profiles contain FA layers (red) below 5 km Above Sea Level (ASL), sometimes mixed with clear-sky layers (white), consistently with *Cesana et al*. [2016] and *Chepfer et al*. [2013]. Figure 3b shows the new flags from the Instant_OPAQ mask, in complement to the Instant_Cloud_OPAQ ones. In this new mask, opaque cloud profiles with no surface echo are now clearly pointed out by their z_opaque layer (green). In all profiles, layers having an SR < 0.06 are classified as Weak_signal (yellow) either when a surface echo or a cloud are detected further down that layer in the profile, meaning that at these layer altitudes, enough laser light is still propagating downward to have sufficient backscatter to retrieve information from the atmospheric layers below. Compared to Figure 3a, this complementary classification (Figure 3b) brings a more coherent spatial structure of atmospheric opacity, since brown and red colors together point out unsounded atmospheric layers, from below the lowest cloud detected to the surface.

We isolated the profile "A" between two black vertical lines near 9.5°N in Figures 3a and 3b. Figure 3c shows its full vertical resolution ATB532 signal in blue and the 480 m vertical resolution SR signal from GOCCP in red. Three vertical lines represent the FA (SR = 0.06), the clear sky (SR = 1.2), and the cloud thresholds (SR = 5). The color boxes on the right show the Instant_OPAQ mask flags, from top to bottom: four levels classified as clear sky (white), four clouds (blue), the z_opaque (green), four Clear_FA (dark brown), and eight FA (red). The ATB532 signal shows no surface echo inside the NSL layer delimited by the dashed grey lines around 0 km asl, which validates its classification as an opaque cloud profile.

Figure 3d shows the "B" profile, near 9.2°N in Figures 3a and 3b. Despite the SR dropping under the FA threshold below 4 km, a clear surface echo is observed in the NSL layer, crossing the SDT. This profile is hence classified as thin cloud, and the weak SR values in the bottom of the profile are flagged as Weak_signal (yellow). In GOCCP v2.9 these weak signal layers in Figure 3d were not distinguished from the FA layers found in Figure 3c.

2.4.2. Southern Ocean Case Study

The second case study is a segment of the 23 November 2007 nighttime orbit (T01-25-08ZN) in the Southern Ocean (Figure 4).

In Figure 4a (Instant_Cloud_OPAQ mask) no FA layer appears at all below the low clouds near 1 km. In Figure 4b (Instant_OPAQ mask), most profiles present a z_opaque level (green), which classifies them as opaque cloud profiles. The "C" profile (near 54.8°S) is detailed in Figure 4c and shows below the lowest cloud at 1 km–1.5 km ASL a steady decrease in the ATB532 signal, with no surface echo in the NSL. The "D" profile (Figure 4d) shows a very similar atmospheric state: high clouds around 6 km and low ones between 1 km and 1.5 km asl. However, an unambiguous surface echo appears in the NSL layer, in spite of a steady decrease in the ATB532 near-surface signal quite similar to the one found in the opaque cloud profile (Figure 4c). Comparing Figures 4c and 4d illustrates why the ATB532 signal must be used at its 30 m full vertical resolution for the surface detection, as the vertically averaged SR profiles in Figures 4c and 4d cannot be distinguished.

3. Adding OPAQ to a Satellite Simulator for Climate Model Evaluation

Adding z_opaque, the opaque cloud cover, and the thin cloud cover diagnostics in the lidar simulator will let us evaluate the opaque and thin clouds representation in climate models by comparing it to the observations. In this section, we describe how the new cloud variables defined above are implemented within the COSP/lidar simulator.

The CFMIP Observation Simulator Package (COSP) [*Bodas-Salcedo et al*., 2011] provides satellite simulators that ensure that comparisons between observations and model output are consistent, by mimicking the clouds that would be observed by different satellites if they were overflying the atmosphere predicted by

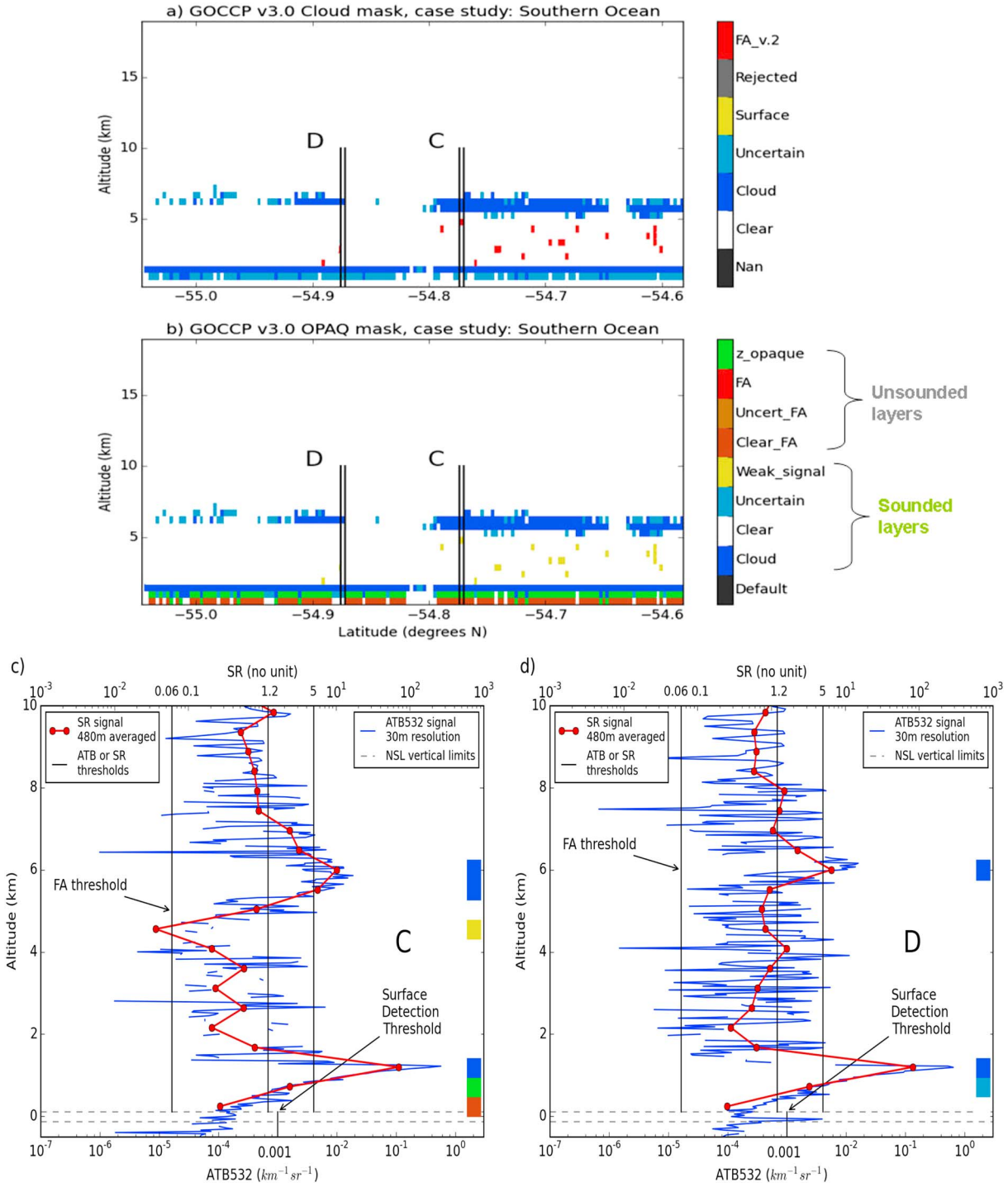

Figure 4. (a–d) Same as Figure 3 but for a low + middle clouds case in the Southern Ocean: C is the opaque cloud profile where the surface echo is not detected (shown in Figure 4c) and D the thin cloud profile where the surface echo is detected (shown in Figure 4d). 23 November 2007, orbit T01-25-08ZN, C is the profile number 52505 (54.7705°S, 17.9771°W) and D is the number 52540 (54.8722°S, 18.0292°W).

a climate model. COSP contains a CALIPSO simulator [*Chepfer et al.*, 2008], which simulates the ATB, the ATB_{mol} (ATB only due to atmospheric molecules at 532 nm), and the SR profiles over 40 vertical levels (480 m vertical resolution) in subgridded climate model outputs, also called atmospheric subcolumns, corresponding to GOCCP-like profiles. Clouds are detected in each profile using $SR > 5$ consistently with CALIPSO-GOCCP. Cloudy subgridded pixels are accumulated over $2° \times 2°$ boxes to build the cloud covers

(low, middle, high, and total) and cloud fraction profiles. COSP/CALIPSO uses a multiple scattering factor of $\eta = 0.7$. The cloud cover is weakly sensitive to this parameter [e.g., *Chepfer et al.*, 2008, 2010, 2013; *Cesana and Chepfer*, 2013]: a difference of less than 1% is observed when changing η from 0.3 to 0.7.

3.1. Implementing the Opaque Cloud Cover, the Thin Cloud Cover, and z_opaque in COSP/CALIPSO

We adapted the COSP/CALIPSO simulator to mimic the opaque and thin cloud covers and the z_opaque that CALIPSO would observe if it was overflying the atmosphere predicted by LMDZ5B [*Hourdin et al.*, 2013b]. The full-year LMDZ5B outputs come from an AMIP-like simulation, without ocean-atmosphere coupling, and SST forced by observations. The implementation of the new opaque variables within COSP/CALIPSO follows the same steps as in the GOCCP v3.0 algorithm described in previous sections.

First, we flag a given atmospheric subcolumn "opaque" if its SR profile contains at least one FA layer ($SR < 0.06$; Appendix C). Because the simulator does not include the surface level, and because unlike the observations it does not include noise, the simulated SR profile always decreases monotonically to zero after passing through an opaque cloud. As a consequence, a unique low SR threshold can be used in the simulator to mimic the OPAQ surface echo detection threshold that is used in GOCCP v3.0 for declaring that a profile is opaque.

If the atmospheric subcolumn has not been flagged opaque, we flag it as "thin" if its SR profile contains at least one cloudy layer ($SR > 5$) and does not contain any FA layer ($SR < 0.06$). A subcolumn is flagged "clear sky" if it does not contain any cloudy or FA layer. The altitude of full opacity z_opaque is then defined in the same way as in the observations: for each opaque cloud subcolumn, z_opaque is the midaltitude of the layer just below the lowest cloud detected.

The calculation of covers is done exactly like in GOCCP (section 2.3). For each day, the sum of opaque cloud, thin cloud, and clear-sky subcolumns gives the total number of profiles at each grid point. Covers are obtained by computing the fraction of each category counts over the total number of profiles. The mean z_opaque at each grid point is, as in GOCCP v3.0, the result of the sum of all z_opaque values in that grid point divided by the number of opaque cloud subcolumns. These additions to COSP give us opaque cloud, thin cloud, and clear-sky covers as well as the mean altitude of opacity as simulator outputs.

4. Results

4.1. Maps of Opaque Cloud Cover, Thin Cloud Cover, and Clear-Sky Cover

We first present maps of opaque cloud cover, thin cloud cover, and clear-sky cover observed by CALIPSO over the period of 2008–2015 (Figures 5a–5c). The annual global mean observed opaque cloud cover is 31%, the thin cloud cover is 35%, and the clear-sky cover is 34%. Opaque clouds are frequent (>40% cover) in regions of deep convection, over the midlatitude oceans, and in stratocumulus regions off the West coasts of the African and the American continents. In contrast, opaque clouds are not frequent (<20% cover) over the extratropical continents, in polar regions, and over the central and western portions of the Atlantic and Pacific oceans.

While the distribution of opaque cloud cover has large regional contrasts, thin cloud cover occurs with a frequency of 30% to 50% over most of the globe. That being said, local minima (10–20%) in thin cloud cover exist over the Middle East, India, and Australia. The largest occurrence frequency (60%) for thin cloud cover occurs in West Antarctica. Thin clouds are also found in regions of tropical deep convection with relatively large occurrence frequency (>40%).

Unsurprisingly, clear sky occurs most frequently in dry and cold regions of the planet. The subsidence regions are often clear, particularly over the Sahara (>70%) and Australian deserts (>60%). Clear sky also commonly occurs (>50%) in the the polar regions.

Next, we compare the observed cover with cover modeled by the LMDZ5B climate model. The model overestimates the observed global mean opaque cloud cover occurrence frequency (38%) but reproduces its main patterns (Figure 5d versus Figure 5a). In the modeled Northern Hemisphere midlatitude storm tracks, the Southern Ocean and the warm pool have substantially more opaque cloud cover than CALIPSO observes. The well-depicted Intertropical Convergence Zone (ITCZ) across the Pacific Ocean that appears in the observations (Figure 5a) is not represented in the model (Figure 5d). Finally, besides the overestimated modeled opaque clouds located over the warm pool (70%) the model represents correctly opaque clouds in both the stratocumulus regions and over the lands where deep convection occurs.

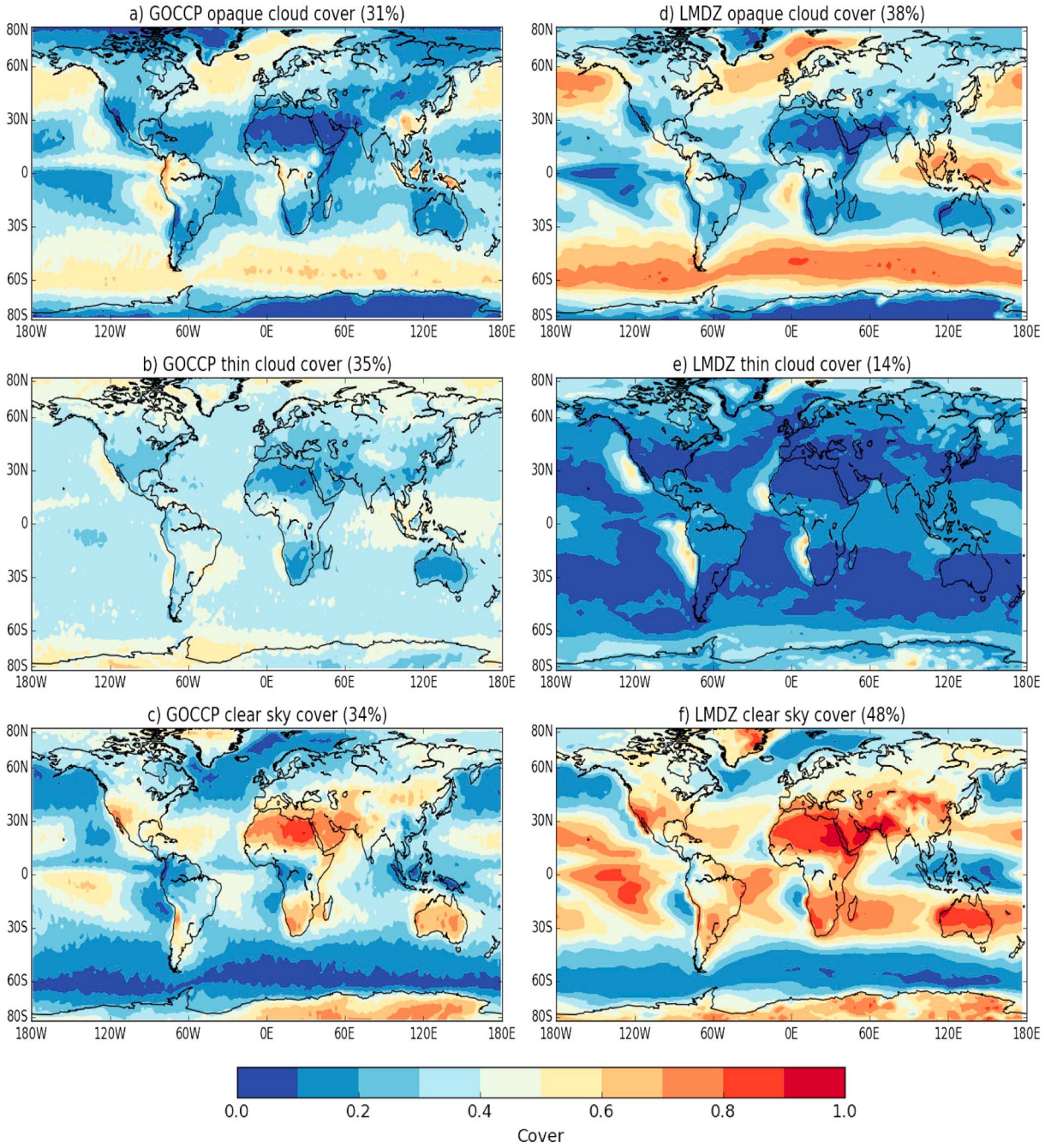

Figure 5. Annual mean GOCCP v3.0 observation (2008–2015) maps of fractional cover for (a) opaque cloud, (b) thin cloud, and (c) clear-sky. (d–f) Same as Figures 5a–5c but for results from the LMDZ5B model (AMIP-like run). In each gridbox the sum of opaque cloud cover, thin cloud cover, and clear-sky cover is one.

In contrast to the opaque cloud cover, the modeled global mean thin cloud cover is largely underestimated (14%) compared to the observations (35%). Figure 5e shows a rather similar geographical distribution of the thin cloud cover for the model compared to the observations (Figure 5b) but with much lower values everywhere except near the poles and the stratocumulus regions. Instead of a uniform 30% of thin clouds across the midlatitudes and the tropics, a 10% value is given by the model. The highest values (40%–50%) of thin clouds are mainly found off the West coasts of the African and the American continents next to the stratocumulus opaque clouds.

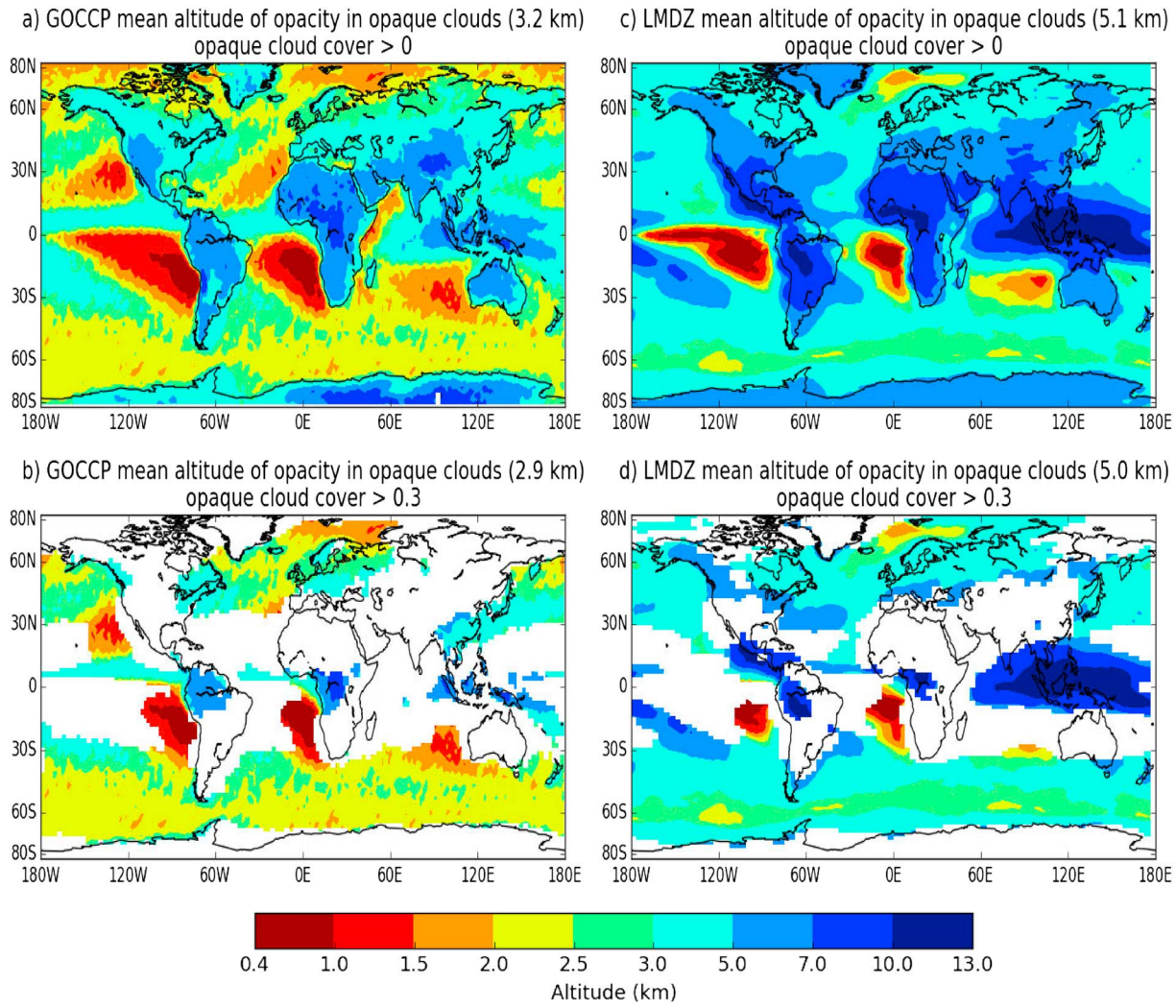

Figure 6. Annual mean GOCCP v3.0 observation (2008–2015) maps of the mean z_opaque, computed over opaque profiles only for (a) opaque cloud cover $>$ 0 and (b) opaque cloud cover $>$ 0.3. (c and d) Same as Figures 6a and 6b but for results from the LMDZ5B model (AMIP-like run).

The global mean clear-sky cover value is significantly larger for the model (48%) than for the observations (34%). High values of clear sky (70%) occur almost all over the globe except in the midlatitude storm tracks, the stratocumulus regions, and where deep convection occurs. The model produces clear sky at the places where thin clouds are observed.

4.2. Maps of z_opaque

The observed patterns over the oceans in Figure 6a illustrate the global atmospheric circulation. The ITCZ and the warm pool (ascending branches of the Hadley cells) show the highest observed mean z_opaque over ocean up to 7 km ASL. In oceanic subsidence regions (descending branches of the Hadley cells) the mean z_opaque is below 2 km. The Southern Ocean shows a rather homogeneous mean z_opaque between 2 and 2.5 km across the entire 40°S–70°S belt. In the Northern Hemisphere midlatitudes, a higher spatial variability is observed because of the strong influence of continents: mean z_opaque ranges between 2 km and 5 km in the storm track and slightly decreases poleward. By keeping only grid points with more than 30% of opaque cloud profiles, Figure 6b highlights the three regions where the opaque cloud effect is going to be the strongest: along the ITCZ (z_opaque $>$ 3 km), in the stratocumulus regions in the subtropics (z_opaque $<$ 2 km), and in the midlatitude storms tracks (2 km $<$ z_opaque $<$ 3 km).

The global mean modeled z_opaque (5.1 km ASL; Figure 6c) is more than 1.5 times higher than the observed one (3.2 km). Z_opaque is too high in the model almost everywhere, except in the opaque stratocumulus

clouds off the West coast of Africa, South America, and Australia, where the mean model z_opaque (~1.5 km) is consistent with observations—likely because the model is able to keep those lower clouds within the boundary layer. Over tropical continents, the model does reproduce high opaque clouds, where deep convection is triggered, but the modeled z_opaque is too high compared to the observations (e.g., 7–13 km instead of 5–9 km). Figure 6d shows that the model roughly reproduces the first-order pattern of z_opaque over the globe. However, the northern subtropics, the ITCZ, and the warm pool patterns could be improved and the model z_opaque is globally too high by a few kilometer compared to observations.

4.3. Link Between the Cloud Radiative Effects and the Opaque Clouds

This section aims to examine the first-order relationships between the cloud variables presented in this paper (opaque cloud cover, thin cloud cover, and z_opaque) and the cloud radiative effect (CRE). The detailed calculations to link z_opaque to the opaque cloud temperature and, ultimately, to the TOA outgoing longwave flux is out of the scope of this paper and will be the subject of a dedicated future paper. The shortwave (SW) and longwave (LW) CRE are defined as

$$\mathrm{CRE}_{\mathrm{SW,\ TOA}} = F^{\uparrow}_{\mathrm{SW,\ TOA}}\_\mathrm{clear\_sky} - F^{\uparrow}_{\mathrm{SW,\ TOA}}\_\mathrm{all\_sky} \quad (3)$$

$$\mathrm{CRE}_{\mathrm{LW,\ TOA}} = F^{\uparrow}_{\mathrm{LW,\ TOA}}\_\mathrm{clear\_sky} - F^{\uparrow}_{\mathrm{LW,\ TOA}}\_\mathrm{all\_sky} \quad (4)$$

where $F^{\uparrow}_{\mathrm{SW,\ TOA}}$_clear_sky and $F^{\uparrow}_{\mathrm{LW,\ TOA}}$_clear_sky are, respectively, the outgoing SW and LW TOA fluxes for the clear-sky atmosphere, and where $F^{\uparrow}_{\mathrm{SW,\ TOA}}$_all_sky and $F^{\uparrow}_{\mathrm{LW,\ TOA}}$_all_sky are the same for an all-sky atmosphere. We compare the CRE with the new cloud variables, first in the observations, then in the model.

a Observations

Figure 7a shows the annual zonal distribution of the cooling of the Earth ($\mathrm{CRE_{SW}}$, blue) due to clouds reflecting the incoming solar radiation back to space. Here we compare the nighttime opaque cloud variables from GOCCP v3.0 to CERES-Energy Balanced and Filled (EBAF) CREs [*Loeb et al.*, 2009]. We hope in the future to expand this comparison to the rest of the diurnal cycle. The zonal mean $\mathrm{CRE_{SW}}$ shown in Figure 7a appears directly anticorrelated (correlation coefficient $R = -0.95$) to the annual zonal opaque cloud cover weighted by the cosine of the latitude (black). The largest contribution to the cooling ($-70\ \mathrm{W\,m^{-2}}$) comes from the persistent Southern Ocean opaque clouds, and the weakest (weaker than $-25\ \mathrm{W\,m^{-2}}$) is observed beyond 65° near both poles. This result is consistent with *Bender et al*. [2011], who focused mainly on stratocumulus clouds and shows that the opaque cloud cover can be considered as a proxy for cloud albedo distribution.

In the longwave, we combined two relevant parameters to approach the $\mathrm{CRE_{LW}}$ shape of Figure 7c (red). On the one hand, z_opaque (Figure 7b) matters because the higher altitude the opacity, the colder temperatures. High z_opaque therefore implies weaker LW emissions. On the other hand, a greater opaque cloud cover will lead to a stronger heating and hence to a weaker LW TOA flux, given the same z_opaque. In order to combine both effects, we computed as a first guess the weighted opacity altitude in each 2° × 2° grid box: Weighted_z_opaque = z_opaque × opaque cloud cover. The shape of the annual zonal Weighted_z_opaque (Figure 7c, black) is very close to the $\mathrm{CRE_{LW}}$ (R = 0.94). As Figure 7c shows, the strongest zonal LW heating from clouds ($40\ \mathrm{W\,m^{-2}}$) occurs in the northern part of the ITCZ where the Weighted_z_opaque is maximum. The Weighted_z_opaque has two local minima in the tropical subsidence (20°S and 25°N) which correspond to the $20\ \mathrm{W\,m^{-2}}$ local minima LW heating from clouds. Interestingly, the northern and southern midlatitudes have similar $\mathrm{CRE_{LW}}$, but those are associated to different types of clouds: the Southern Ocean has a large opaque cloud cover (0.5) associated to a low z_opaque (~2.5 km asl) whereas the northern midlatitudes has a lower opaque cloud cover (0.3) associated to a higher z_opaque (~3.5 km). It is important to note that opaque atmosphere LW heating is not the only cloud-heating mechanism involved here: thin cloud LW heating is also included in the EBAF $\mathrm{CRE_{LW}}$. Nevertheless, since the total $\mathrm{CRE_{LW}}$ seems to be driven primarily by the opaque cloud LW opacity distribution expressed as the Weighted_z_opaque, the thin cloud LW heating appears as a second order term at the global scale.

b Models

In Figure 8 we evaluate if the LMDZ5B model reproduces the observed relationships between our new cloud variables and the CRE. In the SW, the global mean CRE simulated by the model is biased by about $-2\ \mathrm{W\,m^{-2}}$ compared to observations ($-49.0\ \mathrm{W\,m^{-2}}$ instead of $-47.1\ \mathrm{W\,m^{-2}}$). The zonal mean $\mathrm{CRE_{SW}}$ (Figure 8a) shows

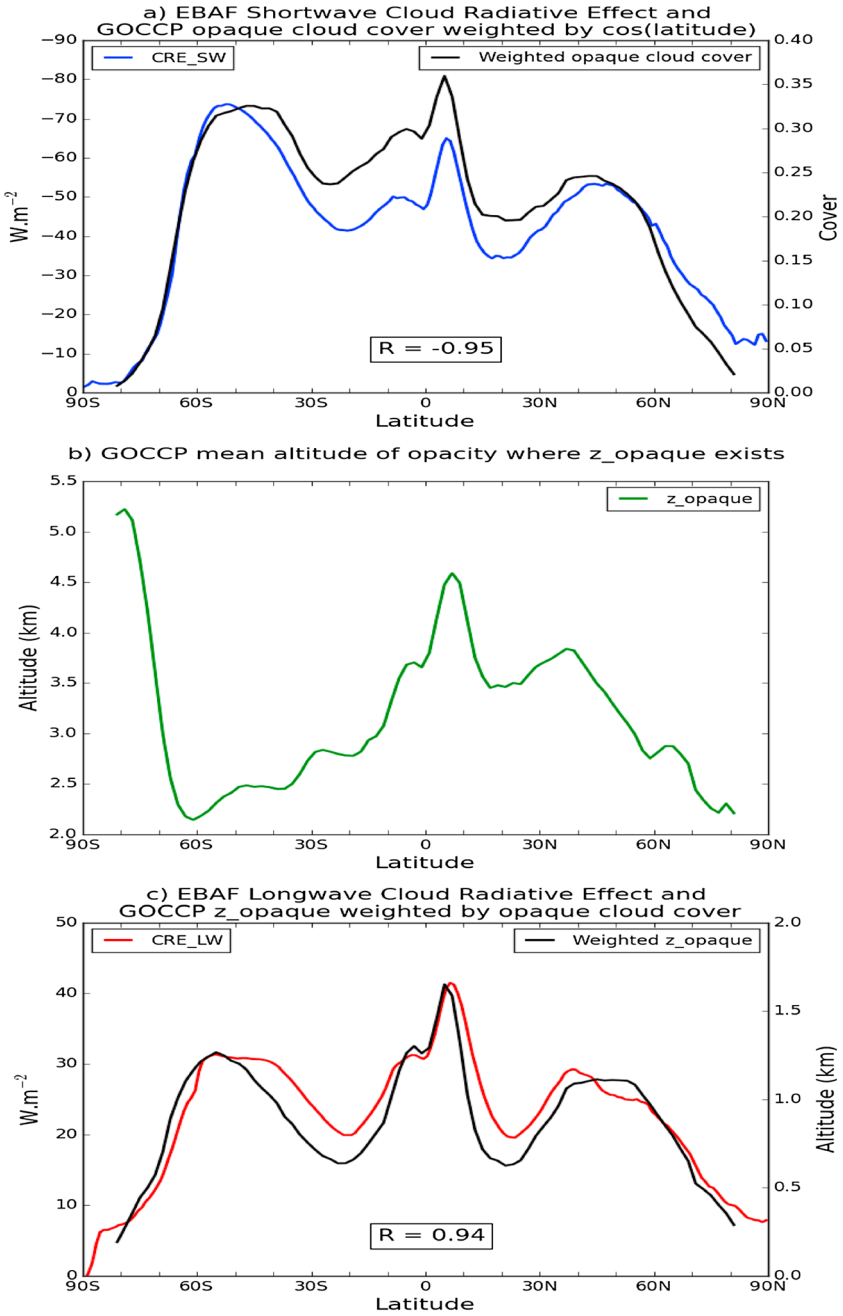

Figure 7. Observed annual zonal means of (a) shortwave cloud radiative effect and opaque cloud cover weighted by the cosine of the latitude, (b) altitude of opacity, and (c) longwave cloud radiative effect and the Weighted_z_opaque. From GOCCP v3.0 and CERES-EBAF, 2008–2015. Weighted_z_opaque = z_opaque × opaque cloud cover.

that the model cool bias comes from the midlatitudes, and more specifically from the Southern Ocean. This strong bias ($-20\,W\,m^{-2}$) is shared by other models [*Kay et al.*, 2012, 2016b; *Bodas-Salcedo et al.*, 2014]. The Southern Ocean CRE_{SW} bias in the model shown in Figure 8a is directly correlated to an opaque cloud cover bias (Figures 8b and 8c) since the correlation between the CRE_{SW} and the opaque cloud cover weighted by the cosine of the latitude is as high in the model as it is in the observations (−0.95). Figures 8a–8c thus suggest that the opaque cloud cover bias alone is sufficient to explain the CRE_{SW} model bias at this scale.

In the LW, the global mean CRE simulated by the model ($25.6\,W\,m^{-2}$) is practically the same than to one given by the observations ($25.8\,W\,m^{-2}$). The model overestimates the CRE_{LW} at the Southern Ocean but is very

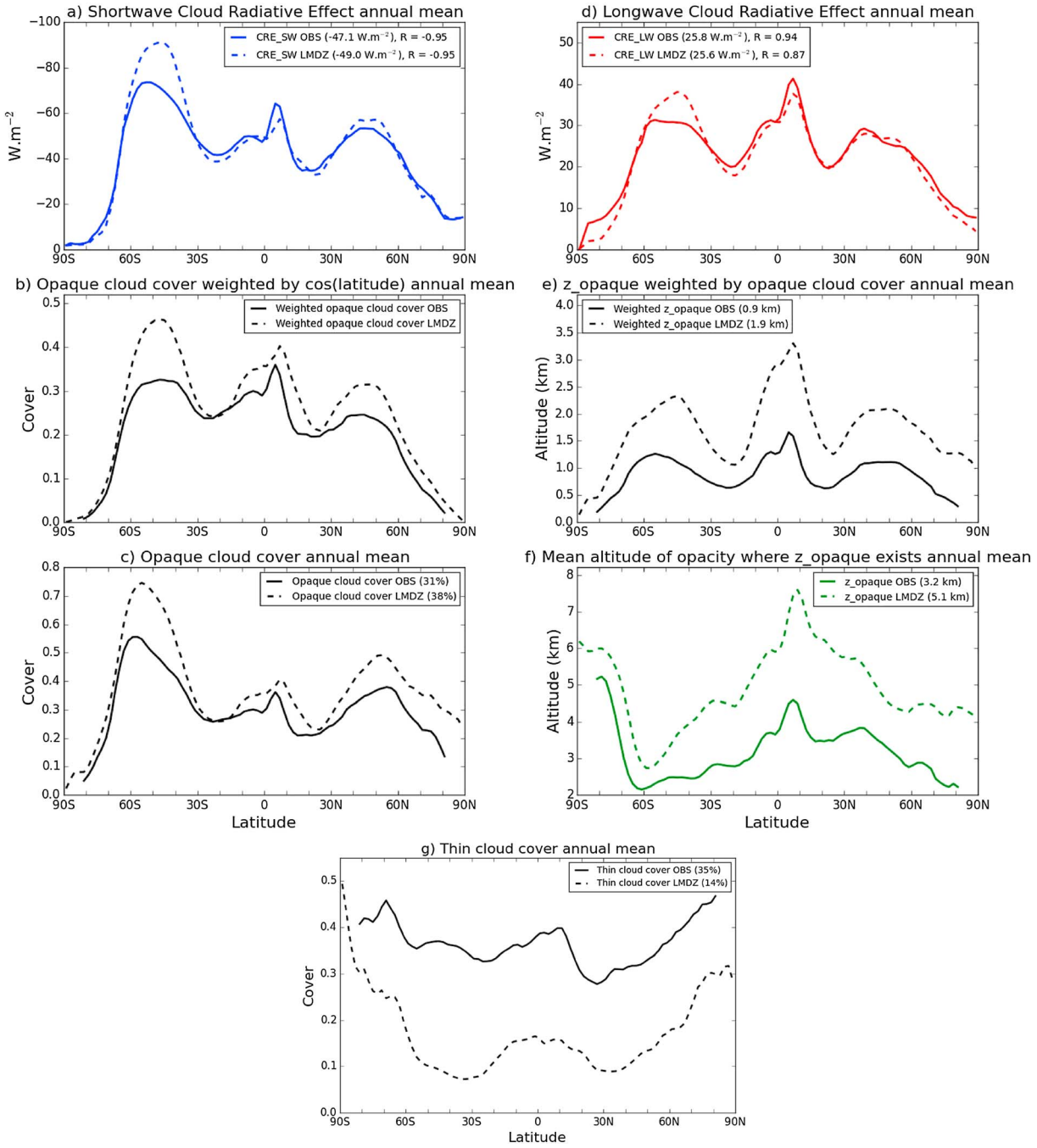

Figure 8. Comparison between the observed and modeled annual zonal means of (a) shortwave cloud radiative effect, (b) opaque cloud cover weighted by the cosine of the latitude, (c) opaque cloud cover, (d) longwave cloud radiative effect, (e) Weighted_z_opaque, (f) altitude of opacity, and (g) thin cloud cover. The observations (solid line) are from CERES-EBAF and CALIPSO GOCCP, and the model (dashed line) is the LMDZ5B.

close to observations at all other latitudes (Figure 8d). It means that the clouds simulated by the model only warm too much the Earth between 35°S and 60°S. Despite the agreement in both modeled and observed CRE_{LW}, the model does not perform as well in reproducing the first-order relationship between the Weighted_z_opaque and the CRE_{LW}: $R = 0.87$ for the model against $R = 0.94$ for the observations. Looking at each term individually (Figures 8c and 8f) suggests that the opaque cloud cover is overestimated by the model compared to observations mainly at the midlatitudes, and z_opaque is overestimated at all latitudes. These two biases should produce a significant positive bias of the model CRE_{LW} at global scale (as suggested

by Figure 8e), but they do not, because they are largely compensated by the thin cloud cover which is underestimated by a factor of 2 to 3 at all latitudes (Figure 8g). In other words, opaque cloud cover is overestimated which implies weaker LW TOA fluxes; opaque clouds are also too high by few kilometer in the model and emit less outgoing LW radiation than they should. These two features increase the CRE_{LW} and warm too much the Earth system. However, both model biases on z_opaque and the opaque cloud cover compensate for the lack of thin clouds in the model (more than half of the thin clouds are missing) that would have contributed to increase the CRE_{LW} if they were properly simulated.

5. Summary

In this paper, we split the atmosphere in three: opaque clouds, thin clouds, and clear sky, using a new algorithm applied to spaceborne lidar observations. The most important results from this study are the following. In global mean, the observed altitude of opacity is 3.2 km and the observed opaque cloud cover is 31%. In the observations, z_opaque weighted by the opaque cloud cover is strongly correlated to the TOA longwave CRE, and the opaque cloud cover is strongly correlated to the TOA shortwave CRE. These correlations show that the three new variables presented in this paper are first-order drivers for radiation. We examined these same relationships in a climate model, using a lidar simulator. We found that the model fairly reproduces the observed relationships, but that a more detailed analysis reveals important first-order error compensations in the modeled clouds. The most striking one is that the model overestimates opaque cloud cover and z_opaque by few kilometers, which should lead to a large radiative bias at the TOA, but the model compensates for this bias by largely underestimating the thin cloud cover.

The results presented in this paper suggest that the new opaque cloud variables are key drivers of the cloud-radiation interactions. These cloud variables present the important advantage of being directly observable at global scale, thanks to spaceborne lidars. In addition to its relevance for radiation, the altitude of opacity is also a new useful direct observational constrain for convection and atmospheric circulation: where z_opaque is significantly too high means that the model transports a significant amount of water too high in the atmosphere. We showed the potential of introducing these opaque cloud diagnostics in climate models by means of the lidar simulator to address further improvements in cloud parameterization, since these new variables appear as major TOA CRE drivers. Using these specific cloud diagnostics would not only help reduce existing biases compared to the observations concerning the Earth's energy budget but also boost confidence in the ability of climate models to correctly foresee the dominant cloud feedback that will drive our future climate. Future work will include a more detailed analysis of the 10 year record of opaque/thin cloud variables collected by CALIPSO and the use of these new diagnostics to evaluate cloud-radiation-circulation interactions in several climate models.

Appendix A: Sensitivity of the Surface Echo Detection to the Near-Surface Layer Thickness

In order to correctly interpret the differences observed between Figures 2a and 2b and in Table 1, figures comparing the 240 m and the 960 m NSL cases are shown. Figures A1a and A1b present the 240 m minus the 960 m distribution maps for, respectively, the no surface echo and the surface echo categories.

The high increase of almost 6% seen in Table 1 for the opaque cloud profile category in the 240 m NSL compared to the 960 m case is located geographically where the positive values are found in Figure A1a. Indeed, reducing the thickness of the NSL can either leave the profile in the same category if ATB_surf_max is the same for both NSL, hence found near the middle of the NSL, or transfer the profile from the detected surface echo category to the opaque cloud one. This latter case happens if ATB_surf_max is both significantly greater than all the other ATB532 values and is away from the middle of the NSL, where the surface echo is supposed to be if the surface elevation is accurate enough. Having this in mind, the averaged +30% values observed in Figure A1a off the West coasts of North and South America, off the West coast of Namibia, the +10% and +20% distributed in the Southern Ocean belt and the Northern Atlantic show a transfer from the detected surface echo cases to the opaque cloud category, with no surface echo at all. This cases can be explained as follows: when looking for ATB_surf_max in the 960 m NSL, a nonnegligible amount of low cloud scenes will make appear this maximum in the upper part of the NSL if no proper and greater surface echo value exists. By keeping only eight layers of 30 m for the NSL, just four above the surface elevation representing

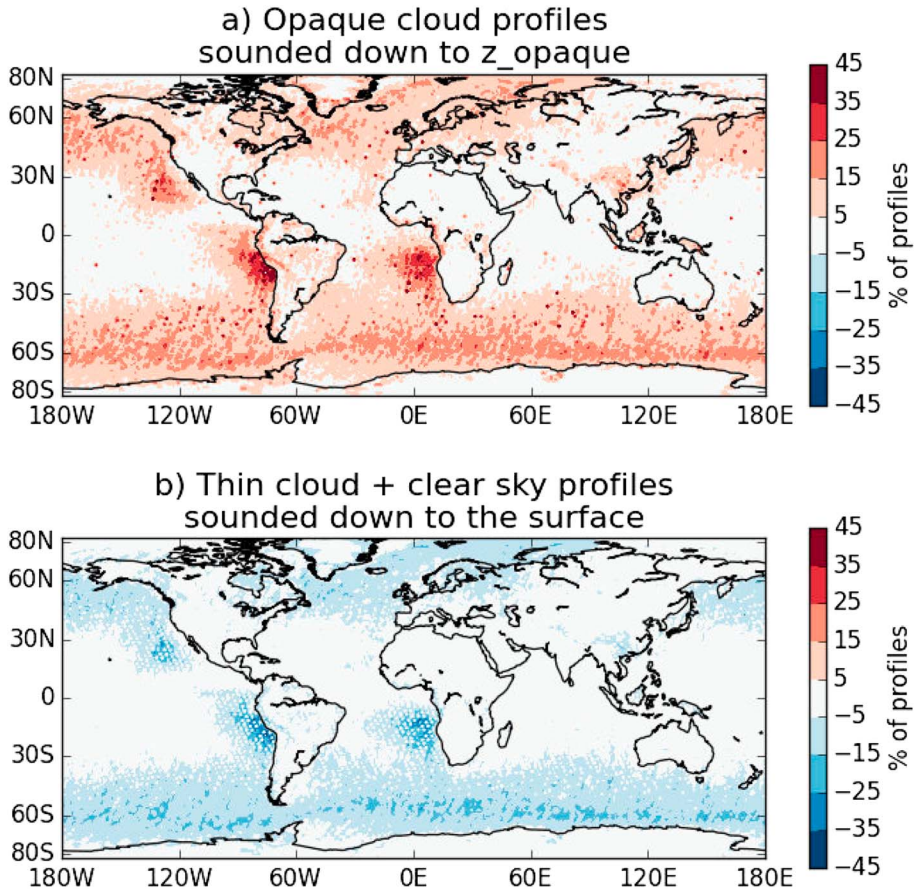

Figure A1. Maps showing the difference in percentage of (a) opaque cloud profiles and (b) thin cloud + clear-sky profiles using a surface detection threshold = 0.001 km^{-1} sr^{-1} for near-surface layer Δh = 240 m case minus Δh = 960 m case, for all 2012 nighttime profiles.

a 120 m thick atmospheric layer, these cases contaminated by low clouds and not detecting the actual surface signal are reduced substantially and more ATB_surf_max below the 0.001 km^{-1} sr^{-1} SDT emerge. This particular case represents the bulk of the 5.8% total increase of the opaque cloud profiles as shown in Table 1. These cases are effectively associated mainly to low clouds as Figure A1a shows high values of increase in the stratocumulus regions, the Northern storm track oceans, and the Southern Ocean belt, all of these regions known for presenting relatively important amounts of low clouds.

In Figure A1a, a few +10% in the Antarctic and Greenland coast lines are associated to decreases of the same amount in Figure A1b. These cases, that can only be observed in polar regions, show us one limit of this simple approach to detect the surface echo signal with a 240 m NSL: since the actual ice or snow surface of the observed scene can differ of a few hundred meters with respect to the surface elevation value in this regions, some previously strong surface echo profiles (ATB_surf_max ~ 2 km^{-1} sr^{-1}) are incorrectly considered as having no surface echo because the Strong surface echo that could be observed within the 960 m NSL is above, below, or at the edges of the 240 m NSL used here to detect the signal. This is the only limitation of this rather simple method, and it justifies our final choice for the OPAQ algorithm in order to make it as accurate and robust as possible. Reducing the number of 30 m layers for the NSL further than eight levels would increase in a nonnegligible way the amount of misclassified profiles in these regions as having no surface echo while actually being detectable ice or snow surfaces.

Appendix B: Description of the OPAQ Products

This section provides a brief presentation of all level 2 and level 3 GOCCP v3.0 products. Level 2 (or orbit files) products refer to information retrieved at the highest GOCCP space and time scales for the 480 m vertically

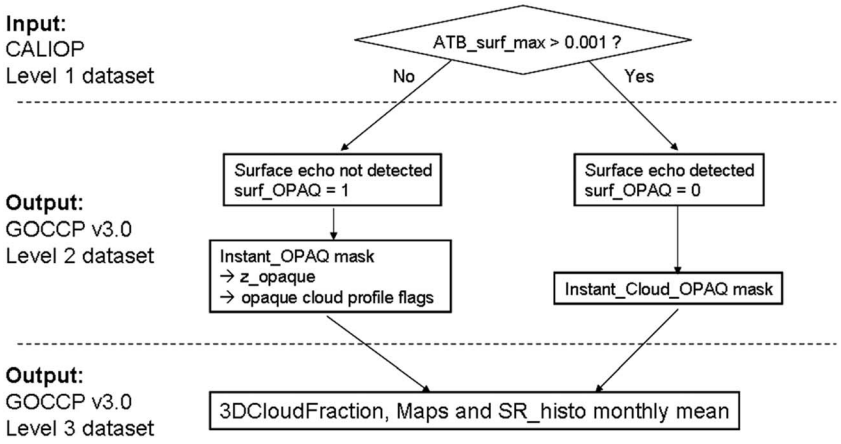

Figure B1. Flow chart showing the main steps and variables of the OPAQ algorithm.

averaged profiles at the 330 m horizontal resolution. Level 3 (or gridded) products are the available variables on a monthly basis on either the 3-D grids or the 2-D maps.

As shown in Figure B1, two new variables are available at the level 2 output. The first one is the surf_OPAQ flag, which has one value per profile and is used to determine whether the profile is classified as opaque

Table B1. GOCCP v3.0 Level 2 Products: Definitions, Characteristics, and Flag Values

Geophysical Quantity	Flag	Description/Fulfilled Conditions	Flag Value
	For Each Profile (surf_OPAQ Variable)		
Surface echo detected	Thin cloud or clear-sky profile	ATB_surf_max $>$ 0.001	0
Surface echo not detected	Opaque cloud profile	ATB_surf_max $<$ 0.001	1
Rejected profile	Undefined	Level 1 surface elevation not available	−9999
	Cloud Mask for Each 480 m Layer (Instant_Cloud_OPAQ Variable) All Profiles		
Not available value	Nan	SR = −9999	1
Clear sky	Clear	0.06 $<$ SR $<$ 1.2	2
Cloud detected	Cloud	SR $>$ 5	3
Aerosol/faint cloud	Uncertain	1.2 $<$ SR $<$ 5	4
Surface detection	Surface	SR = −888	6
Rejected value	Rejected	SR = −777	7
Fully attenuated (FA)	FA_v.2	SR $<$ 0.06 (FA threshold = 0.06 instead of 0.01)	8
	OPAQ Mask for Each 480 m Layer (Instant_OPAQ Variable) All Profiles		
All other cases	Default	None of the cases described below	0
Highest cloud detected	Uppermost_cloud_layer	SR $>$ 5 AND at least another cloud below AND no cloud above	1
Middle cloud detected	In_cloud_layer	SR $>$ 5 AND at least another cloud below AND at least another cloud above	2
Lowest cloud detected	Undermost_cloud_layer	Last SR $>$ 5 from TOA to the surface	3
	Profiles Sounded Down to the Surface (Thin Cloud and Clear-Sky Profiles)		
Clear sky	Clear	0.06 $<$ SR $<$ 1.2	4
Aerosol/faint cloud	Uncertain	1.2 $<$ SR $<$ 5	5
Weak signal	Weak_signal	SR $<$ 0.06	6
	Profiles Sounded Down to z_opaque (Opaque Cloud Profiles)		
Clear sky	Clear	0.06 $<$ SR $<$ 1.2 **AND** above lowest cloud	4
Aerosol/faint cloud	Uncertain	1.2 $<$ SR $<$ 5 **AND** above lowest cloud	5
Weak signal above lowest cloud	Weak_signal	SR $<$ 0.06 **AND** above lowest cloud	6
Clear sky-FA	Clear_FA	0.06 $<$ SR $<$ 1.2 **AND** below lowest cloud	7
Uncertain-FA	Uncert_FA	1.2 $<$ SR $<$ 5 **AND** below lowest cloud	8
Fully attenuated	FA	SR $<$ 0.06 **AND** below lowest cloud	9
Full opacity altitude	z_opaque	First layer just below the lowest cloud detected	10

Table B2. GOCCP v3.0 Level 3 Monthly Products: Definitions and Variable Names

Geophysical Quantity	Variable Name
3-D Fractions (CF3D)	
All atmosphere	
Total cloud fraction	clcalipso
Total clear fraction	clrcalipso
Total uncertain fraction	uncalipso
Atmosphere Sounded Down to the Surface (Thin Cloud and Clear-Sky Profiles)	
Cloud fraction	clcalipso_notopaque
Clear fraction	clrcalipso_notopaque
Uncertain fraction	uncalipso_notopaque
Atmosphere Sounded Down to z_opaque (Opaque Cloud Profiles)	
Cloud fraction	clcalipso_opaque
Clear fraction	clrcalipso_opaque
Uncertain fraction	uncalipso_opaque
Z_opaque fraction	calipsozopaque
2-D Maps	
All Atmosphere	
Total cloud cover	cltcalipso
Total clear-sky cover	clccalipso
Atmosphere Sounded Down to the Surface (Thin Cloud and Clear-Sky Profiles)	
Total thin cloud cover	cltcalipso_thin
Total thin cloud cover + total clear-sky cover	calipso_notopaque
Atmosphere Sounded Down to z_opaque (Opaque Cloud Profiles)	
Total opaque cloud cover	cltcalipso_opaque
Mean z_opaque altitude	zopaque
SR Histograms	
All Atmosphere	
Lidar Scattering Ratio CFAD (532 nm) occurrences	cfad_lidarsr532_Occ
Atmosphere Sounded Down to the Surface (Thin Cloud and Clear-Sky Profiles)	
Lidar Scattering Ratio CFAD (532 nm) occurrences	cfad_lidarsr532_Occ_notopaque
Atmosphere Sounded Down to z_opaque (Opaque Cloud Profiles)	
Lidar Scattering Ratio CFAD (532 nm) occurrences	cfad_lidarsr532_Occ_opaque

cloud or not. The second variable is the Instant_OPAQ mask which gathers all the information related to the OPAQ algorithm. The instant_OPAQ mask has the same dimension than the GOCCP v2.9 Instant_Cloud legacy mask (number of profiles per orbit times 40 altitude levels), this latter being slightly modified in GOCCP v3.0 (Instant_Cloud_OPAQ): the fully attenuated SR threshold which used to be at SR = 0.01 is now set at SR = 0.06 (Figure C1). Detailed information on flag values and the conditions needed for each variable to be declared are presented in Table B1.

Table B2 summarizes all the available variables of GOCCP v3.0 level 3 output. It is important to note that the difference between thin cloud + clear-sky profiles and opaque cloud profiles allows to study the different 3-D or 2-D spatial distributions of these two complementary portions of the atmosphere, the one sounded down to the surface and the one only sounded partially down to z_opaque. For instance, for the 3-D gridded variables, besides the GOCCP v2.9 cloud fraction, there also is the thin cloud fraction, the opaque cloud fraction, and the z_opaque fraction of occurrence. For the 2-D variables, besides the GOCCP v2.9 all cloud cover and clear-sky cover, there also is the opaque cloud cover, the thin cloud cover, and the nonopaque cover (thin cloud cover + clear-sky cover). The last 2-D variable is z_opaque which does not represent an occurrence cover information like the other 2-D variables but the mean opacity altitude computed over opaque cloud profiles only. The information concerning on which fraction of the total number of profiles in a grid point the mean z_opaque value is calculated is given by the opaque cloud cover. The existence of all these different subsets of monthly gridded data explains the important amount of available variables, which allows the user to easily and directly get to the geophysical field of interest.

Appendix C: Changing the Fully Attenuated Threshold in GOCCP

Figure C1 shows the distribution of SR values below the lowest cloud detected in all nighttime 2012 opaque cloud profiles from GOCCP v3.0. This figure exhibits a bimodal distribution in which the lowest mode

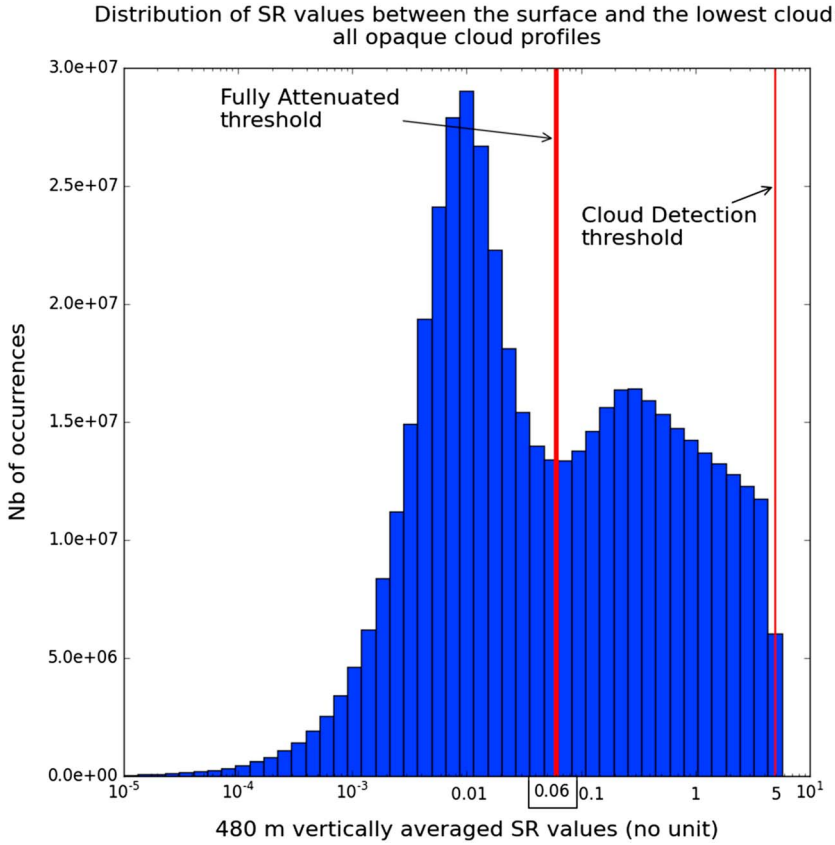

Figure C1. Distribution of SR values for 480 m vertically averaged atmospheric layers located within the lidar unsounded layers: between the lowest cloud detected (SR > 5) and the surface, for all nighttime 2012 opaque cloud profiles only.

represents typical SR values of FA atmospheric layers in observations. The highest mode represents the sum of the multiple scattering signal of the lidar from these highly reflective opaque clouds and of transition SR values associated to the vertical averaging over the 480 m thick layers. Since we are not able to access to the shape of the higher end of the FA mode distribution from the observations, we choose SR = 0.06 (local minimum in Figure C1) as the FA threshold to determine when an atmospheric layer is considered as FA. This analysis allows us to update the FA threshold in GOCCP v3.0 level 2 products (the FA threshold used to be at SR = 0.01 for GOCCP v2.9) and to use this same threshold to determine when a COSP subcolumn atmospheric layer is FA (SR < 0.06).

Acknowledgments
The authors would like to thank NASA, CNES, Icare, and Climserv for giving access to the CALIOP data. Special thanks are due to Climserv for computing resources which let us perform all the data analysis and to produce this new version of the GOCCP product. This work was supported by CNES and NASA grant 12-CCST10-0095. The GOCCP v3.0 products presented in this article are available online through the GOCCP website (http://climserv.ipsl.polytechnique.fr/cfmip-obs/Calipso_goccp.html). The new diagnostics will be available in COSP V2. Thanks are due to the two anonymous reviewers who helped to significantly improve this manuscript.

References

Bender, F. A. M., R. J. Charlson, A. M. Ekman, and L. V. Leahy (2011), Quantification of monthly mean regional-scale albedo of marine stratiform clouds in satellite observations and GCMs, *J. Appl. Meteorol. Climatol.*, *50*(10), 2139–2148.

Bodas-Salcedo, A., M. J. Webb, M. E. Brooks, M. A. Ringer, K. D. Williams, S. F. Milton, and D. R. Wilson (2008), Evaluating cloud systems in the Met Office global forecast model using simulated CloudSat radar reflectivities, *J. Geophys. Res.*, *113*, D00A13, doi:10.1029/2007JD009620.

Bodas-Salcedo, A., et al. (2011), COSP: Satellite simulation software for model assessment, *Bull. Am. Meteorol. Soc.*, *92*(8), 1023–1043.

Bodas-Salcedo, A., K. D. Williams, M. A. Ringer, I. Beau, J. N. Cole, J. L. Dufresne, T. Koshiro, B. Stevens, Z. Wang, and T. Yokohata (2014), Origins of the solar radiation biases over the Southern Ocean in CFMIP2 models, *J. Clim.*, *27*(1), 41–56.

Bony, S., et al. (2006), How well do we understand and evaluate climate change feedback processes?, *J. Clim.*, *19*(15), 3445–3482.

Boucher, O., et al. (2013), Clouds and aerosols, in *Climate Change 2013: The Physical Science Basis*, *Contribution of Working Group I to the Fifth Assessment Report of the Intergovernmental Panel on Climate Change (pp. 571–657)*, Cambridge Univ. Press, Cambridge.

Cesana, G., and H. Chepfer (2012), How well do climate models simulate cloud vertical structure? A comparison between CALIPSO-GOCCP satellite observations and CMIP5 models, *Geophys. Res. Lett.*, *39*, L20803, doi:10.1029/2012GL053153.

Cesana, G., and H. Chepfer (2013), Evaluation of the cloud thermodynamic phase in a climate model using CALIPSO-GOCCP, *J. Geophys. Res. Atmos.*, *118*, 7922–7937, doi:10.1002/jgrd.50376.

Cesana, G., et al. (2016), Using in-situ airborne measurements to evaluate three cloud phase products derived from CALIPSO, *J. Geophys. Res. Atmos.*., *121*, 5788–5808, doi:10.1002/2015JD024334.

Chepfer, H., S. Bony, D. Winker, M. Chiriaco, J. L. Dufresne, and G. Sèze (2008), Use of CALIPSO lidar observations to evaluate the cloudiness simulated by a climate model, *Geophys. Res. Lett.*, *35*, L15704, doi:10.1029/2008GL034207.

Chepfer, H., S. Bony, D. Winker, G. Cesana, J. L. Dufresne, P. Minnis, C. J. Stubenrauch, and S. Zeng (2010), The GCM-Oriented CALIPSO Cloud Product (CALIPSO-GOCCP), *J. Geophys. Res.*, *115*, D00H16, doi:10.1029/2009JD012251.

Chepfer, H., G. Cesana, D. Winker, B. Getzewich, M. Vaughan, and Z. Liu (2013), Comparison of two different cloud climatologies derived from CALIOP-attenuated backscattered measurements (Level 1): The CALIPSO-ST and the CALIPSO-GOCCP, *J. Atmos. Oceanic Technol.*, *30*(4), 725–744.

Chepfer, H., V. Noel, D. Winker, and M. Chiriaco (2014), Where and when will we observe cloud changes due to climate warming?, *Geophys. Res. Lett.*, *41*, 8387–8395, doi:10.1002/2014GL061792.

English, J. M., J. E. Kay, A. Gettelman, X. Liu, Y. Wang, Y. Zhang, and H. Chepfer (2014), Contributions of clouds, surface albedos, and mixed-phase ice nucleation schemes to Arctic radiation biases in CAM5, *J. Clim.*, *27*(13), 5174–5197.

Hourdin, F., et al. (2013b), LMDZ5B: The atmospheric component of the IPSL climate model with revisited parameterizations for clouds and convection, *Clim. Dyn.*, *40*(9–10), 2193–2222.

Kato, S., S. Sun-Mack, W. F. Miller, F. G. Rose, Y. Chen, P. Minnis, and B. A. Wielicki (2010), Relationships among cloud occurrence frequency, overlap, and effective thickness derived from CALIPSO and CloudSat merged cloud vertical profiles, *J. Geophys. Res.*, *115*, D00H28, doi:10.1029/2009JD012277.

Kay, J. E., K. Raeder, A. Gettelman, and J. Anderson (2011), The boundary layer response to recent Arctic sea ice loss and implications for high-latitude climate feedbacks, *J. Clim.*, *24*, 428–447.

Kay, J. E., et al. (2012), Exposing global cloud biases in the Community Atmosphere Model (CAM) using satellite observations and their corresponding instrument simulators, *J. Clim.*, *25*(15), 5190–5207.

Kay, J. E., L. Bourdages, H. Chepfer, N. Miller, A. Morrison, V. Yettella, and B. Eaton (2016a), Evaluating and improving cloud phase in the Community Atmosphere Model version 5 using spaceborne lidar observations, *J. Geophys. Res. Atmos.*, *121*, 4162–4176, doi:10.1002/2015JD024699.

Kay, J. E., C. Wall, V. Yettella, B. Medeiros, C. Hannay, P. Caldwell, and C. Bitz (2016b), Global climate impacts of fixing the Southern Ocean shortwave radiation bias in the Community Earth System Model, *J. Clim.*, *29*, 4617–4636, doi:10.1175/JCLI-D-15-0358.

Klein, S. A., and C. Jakob (1999), Validation and sensitivities of frontal clouds simulated by the ECMWF model, *Mon. Weather Rev.*, *127*(10), 2514–2531.

Konsta, D., H. Chepfer, and J. L. Dufresne (2012), A process oriented characterization of tropical oceanic clouds for climate model evaluation, based on a statistical analysis of daytime A-train observations, *Clim. Dyn.*, *39*(9-10), 2091–2108.

Leahy, L. V., R. Wood, R. J. Charlson, C. A. Hostetler, R. R. Rogers, M. A. Vaughan, and D. M. Winker (2012), On the nature and extent of optically thin marine low clouds, *J. Geophys. Res.*, *117*, D22201, doi:10.1029/2012JD017929.

Loeb, N. G., B. A. Wielicki, D. R. Doelling, G. L. Smith, D. F. Keyes, S. Kato, N. Manalo-Smith, and T. Wong (2009), Toward optimal closure of the Earth's top-of-atmosphere radiation budget, *J. Clim.*, *22*(3), 748–766.

Marchand, R., J. Haynes, G. G. Mace, T. Ackerman, and G. Stephens (2009), A comparison of simulated cloud radar output from the multiscale modeling framework global climate model with CloudSat cloud radar observations, *J. Geophys. Res.*, *114*, D00A20, doi:10.1029/2008JD009790.

Martins, E., V. Noel, and H. Chepfer (2011), Properties of cirrus and subvisible cirrus from nighttime Cloud-Aerosol Lidar with Orthogonal Polarization (CALIOP), related to atmospheric dynamics and water vapor, *J. Geophys. Res.*, *116*, D02208, doi:10.1029/2010JD014519.

Nam, C., S. Bony, J. L. Dufresne, and H. Chepfer (2012), The 'too few, too bright' tropical low-cloud problem in CMIP5 models, *Geophys. Res. Lett.*, *39*, L21801, doi:10.1029/2012GL053421.

Taylor, K. E., M. Crucifix, P. Braconnot, C. D. Hewitt, C. Doutriaux, A. J. Broccoli, J. F. B. Mitchell, and M. J. Webb (2007), Estimating shortwave radiative forcing and response in climate models, *J. Clim.*, *20*(11), 2530–2543.

Taylor, K. E., R. J. Stouffer, and G. A. Meehl (2012), An overview of CMIP5 and the experiment design, *Bull. Am. Meteorol. Soc.*, *93*(4), 485–498.

Vaughan, M. A., K. A. Powell, D. M. Winker, C. A. Hostetler, R. E. Kuehn, W. H. Hunt, B. J. Getzewich, S. A. Young, Z. Liu, and M. J. McGill (2009), Fully automated detection of cloud and aerosol layers in the CALIPSO lidar measurements, *J. Atmos. Oceanic Technol.*, *26*(10), 2034–2050.

Webb, M. J., et al. (2006), On the contribution of local feedback mechanisms to the range of climate sensitivity in two GCM ensembles, *Clim. Dyn.*, *27*(1), 17–38.

Winker, D. M., M. A. Vaughan, A. Omar, Y. Hu, and K. A. Powell (2009), Overview of the CALIPSO mission and CALIOP data processing algorithms, *J. Atmos. Oceanic Technol.*, *26*, 2310–2323.

Yoshida, R., H. Okamoto, Y. Hagihara, and H. Ishimoto (2010), Global analysis of cloud phase and ice crystal orientation from Cloud-Aerosol Lidar and Infrared Pathfinder Satellite Observation (CALIPSO) data using attenuated backscattering and depolarization ratio, *J. Geophys. Res.*, *115*, D00H32, doi:10.1029/2009JD012334.